Acta Geochim (2018) 37(5):715–733
https://doi.org/10.1007/s11631-017-0254-3

ORIGINAL ARTICLE

Geochemistry of the Palaeo–Mesoproterozoic Tadpatri shales, Cuddapah basin, India: implications on provenance, paleoweathering and paleoredox conditions

Rahul Mitra[1] · Gopal Chakrabarti[2] · Debasish Shome[1]

Received: 22 September 2017 / Revised: 26 October 2017 / Accepted: 24 November 2017 / Published online: 5 December 2017

Abstract The Palaeo–Mesoproterozoic Tadapatri formation of the Cuddapah basin is comprised of clastic sedimentary rocks with minor carbonates and mafic–ultramafic sill bodies. Geochemistry of the shale is used to study the provenance, paleoweathering and paleoredox conditions of this Tadpatri formation in order to better understand the development of the Cuddapah basin during Palaeo–Mesoproterozoic time. The higher CIA (average 74.39), PIA (average 85.94) and CIW (average 87.59) values of the Tadpatri shales suggest intensely weathered sources. Higher Al_2O_3/TiO_2 (average 30.78) and LREE/HREE ratio (average 8.80) with negative europium anomaly indicate derivation of the clastic sediments from a felsic source rock. The geochemical parameters like U, U/Th, Cu/Zn, Ni/Co, V/Cr ratios reveal that the Tadpatri shales are mainly deposited in an oxic condition.

Keywords Tadpatri · Provenance · Paleoweathering · Paleoredox · Geochemistry

1 Introduction

The intracratonic Cuddapah basin of Peninsular Indian Shield is considered as the second largest Purana basin of India (Kale 1991). A sequence of thermal upwarping and rifting with crustal thinning leads to the formation of Cuddapah basin over the Eastern Dharwar Craton (Nagaraja Rao et al. 1987; Mishra 2011). However, there is another school of thought that stipulates that the subduction of the oceanic crust in western direction beneath the Dharwar Craton led to the formation of back-arc (extensional) Cuddapah basin at nearly 2000 Ma (Absar et al. 2016). Sedimentation within the Cuddapah basin is represented by four different cycles viz. Papaghni cycle, Chitravati cycle, Srisailam cycle, and the Kurnool cycle, which are episodically interrupted by basin-wide unconformities (Saha and Tripathy 2012). The Chitravati cycle is predominantly composed of Pulivendla, Tadpatri and Gandikota formation from base to top. Therefore, the Tadpatri formation is sandwiched between Pulivendla and Gandikota formation and dominantly composed of mixed clastic-carbonate group of rocks with intruded sill bodies at different stratigraphic levels (Nagaraja Rao et al. 1987; Patranabis-Deb et al. 2012).

The geochemistry of clastic rocks plays an important role in depicting the nature of the provenance, the weathering history of the source area, and the paleooxidation conditions during deposition, which are further used to elucidate the evolution of the ancient depositional basin (Cullers 1995; Cullers and Podkovyrov 2000; Armstrong-Altrin et al. 2004, 2012; Nagarajan et al. 2007; Mir 2015). Among clastic sedimentary rocks, shale is most frequently used to study provenance, paleoweathering, and paleoredox conditions because of its abundance and well homogenization character (Pettijohn 1975; Mir 2015).

Earlier works on the Tadpatri formation essentially focus on the geochemistry of carbonate and mafic–ultramafic rocks, which mainly reflects the depositional environment of Tadpatri stromatolite as well as the depositional age of this formation (Murthy et al. 1987; Nagaraja Rao et al. 1987; Zachariah et al. 1999; Anand et al. 2003;

✉ Rahul Mitra
rahul.swpe@gmail.com

[1] Department of Geological Sciences, Jadavpur University, Kolkata 700032, India

[2] Education Directorate, Government of West Bengal, Kolkata 700091, India

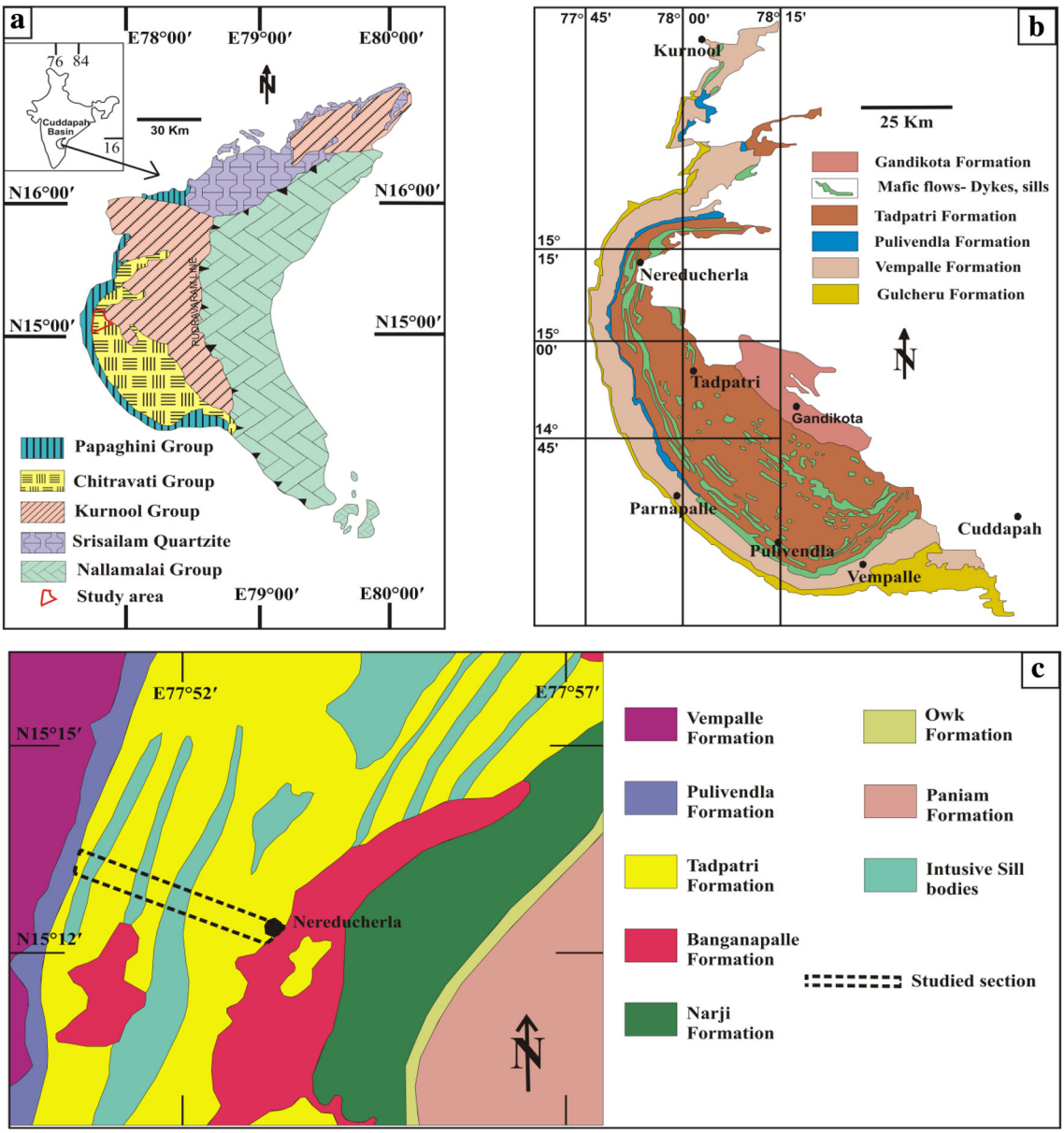

Fig. 1 Geological maps of the study area **a** Generalized geological map of the Cuddapah basin (modified after Geological survey of India 1:2 000 000 map, 1998); **b** Geological map of western Cuddapah basin showing the lower Cuddapah group of rocks (after Nagraja Rao et al. 1987; Saha and Tripathy 2012); **c** North-western part of Cuddapah basin showing location of the measured section investigated in this study (modified after Survey of India Quadrangle map number 57E, 1981; 1:250 000)

French et al. 2008; Khelen et al. 2017). To date, however, there have been no studies conducted on the Tadptari formation rocks (clastic) to depict its provenance, tectonic setting, source rock weathering and paleoredox condition. Therefore, this work, for the first time, sets its objective to examine the provenance, paleoweathering, and paleoenvironmental set up of Tadpatri formation in order to better understand the development of Cuddapah basin during Palaeo–Mesoproterozoic time.

2 Geological setting

The Cuddapah basin preserves nearly 12 km of Late Palaeoproterozoic to Neoproterozoic sedimentary and volcanic strata which are lithostratigraphically divided into the Cuddapah Supergroup and the Kurnool Group (Saha and Tripathy 2012). The Cuddapah Supergroup is unconformably resting over the Eastern Dharwar Craton, which is essentially composed of Tonalite–Trondhjemite–Granodiorite gneisses, greenstone belts with fewer amounts of mafic dykes (Nagaraja Rao et al. 1987). Cuddapah

Supergroup consists of Papaghni, Chitravati, Nallamalai Groups and Srisailam formation from base to top (Fig. 1a and Table 1; Saha and Tripathy 2012). Each of the group is separated by regional unconformities and composed with clastic as well as non-clastic group of rocks which reflects a gross fining upward succession in a shallow marine shelfal set-up (Patranabis-Deb et al. 2012).

The second oldest group within this Cuddapah Supergroup is the Chitravati, mainly exposed in the western part of the basin and consists with Pulivendla, Tadpatri, Gadikota formation from base to top (Fig. 1b). Tadpatri formation principally consists with a large variety of shale (siliciclastic, calcareous, ferruginous chert and jasper bearing), limestone and quartzite. Limestone units are

Table 1 Stratigraphy of the Cuddapah **Basin** (after Nagaraja Rao et al. 1987)

Group		Formation	Lithology	Age
	Kurnool	Nandyal (50-100 m)	Shale/Limestone	Neoproterozoic
		Koilkuntala (15-50 m)	Limestone with shale	
		Paniam (10-35 m)	Quartzite	
		Owk (10-15 m)	Shale	
		Narji (100-200 m)	Massive Limestone, Flaggy Limestone	
		Banganapalli (10-15 m)	Quartzite with conglomerate	
------Unconformity------				
Cuddapah Supergroup		Srisailam (300 m)	Pebbly grit,Quartzite, Heterolithic Shales and stone	Mesoproterozoic
	------Unconformity------			
	Nallamalai	Cumbum (~ Pullampet Shale) (2000 m)	Shale, Dolomitic limestone, Quartzite	
		Bairenkonda (~ Nagari Quartzite) (5500 m)	Pebbly grit,Quartzite, Heterolithic Shales and stone	
	------Unconformity------			
	Chitravati	Gandikota (300 m)	Quartzite, Pebble beds	Mesoproterozoic
		Tadpatri (4600 m)	Shale, Quartzite, Stromatolitic dolomite with mafic flows, Sills and Dykes	
		Pulivendla (1-75 m)	Conglomerate, Quartzite	
	------Unconformity------			
	Papaghni	Vempalle (1900 m)	Stromatolitic dolomite, Shale, Basic flows and intrusive	Palaeoproterozoic
		Gulcheru (30-210 m)	Conglomerate, Feldspathic sandstone and quartzite	
------Unconformity------				
Dharwar Craton				Archean

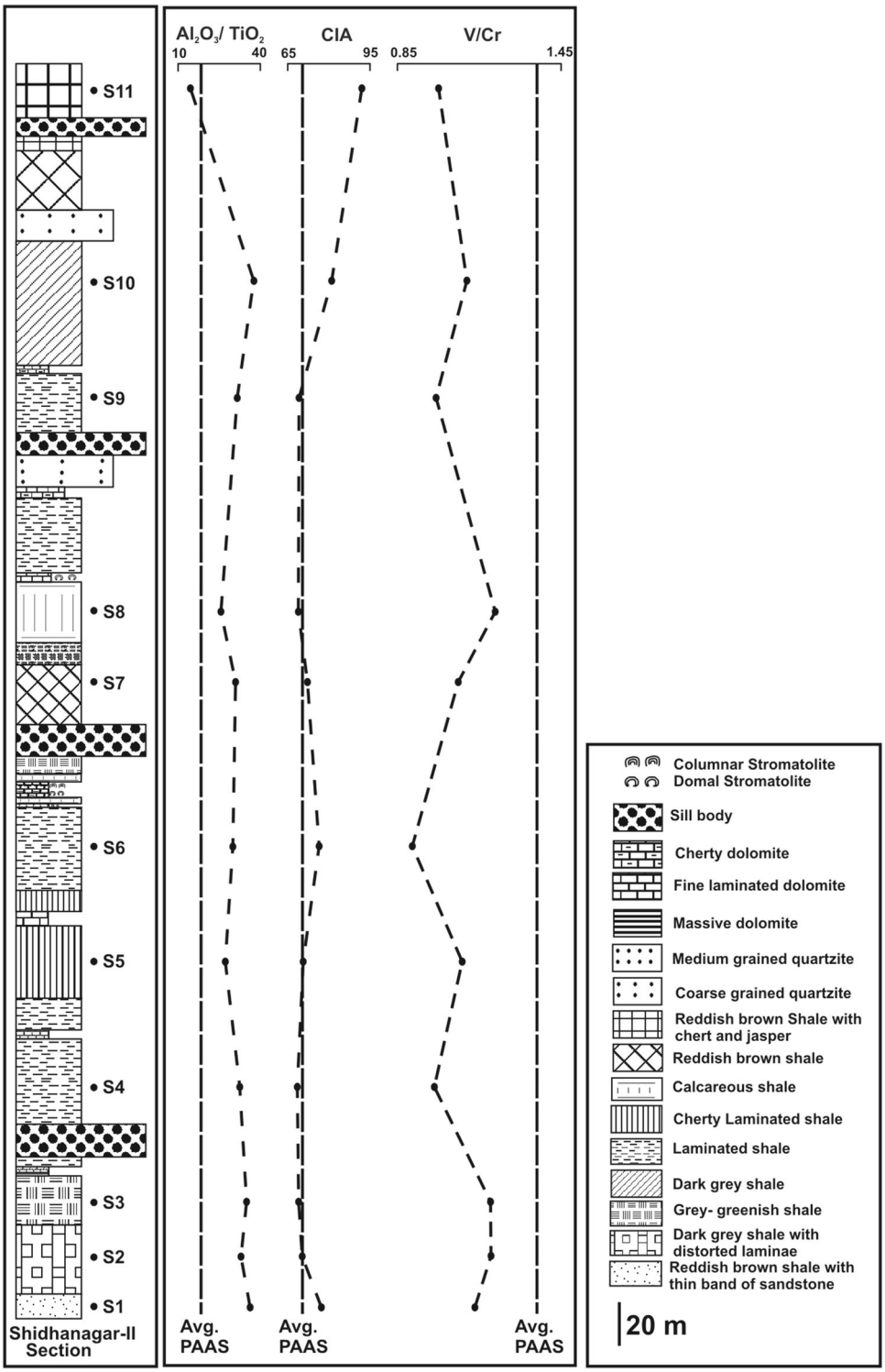

Fig. 2 Litholog showing measured stratigraphic section with the positions of the samples collection. Al_2O_3/TiO_2, CIA, V/Cr values of the Tadpatri shales showing their vertical variation alongside with the average PAAS value (Reproduced with permission from Taylor and McLennan 1985)

thinly laminated to domal and columnar stromatolite bearing (Patranabis-Deb et al. 2012). Stromatolites have low amplitutde hemispheroidal forms; smaller laterally linked hemispheroids are also common (Sharma and Shukla 2003). There are also many mafic–ultramafic sill bodies with variable thickness developed at different stratigraphic positions within the Tadpatri formation. The lithology, sedimentary structures and microbialites morphology clearly demonstrate that the deposition of Tadpatri formation is in a shallow marine shelfal condition (Patranabis-Deb et al. 2012).

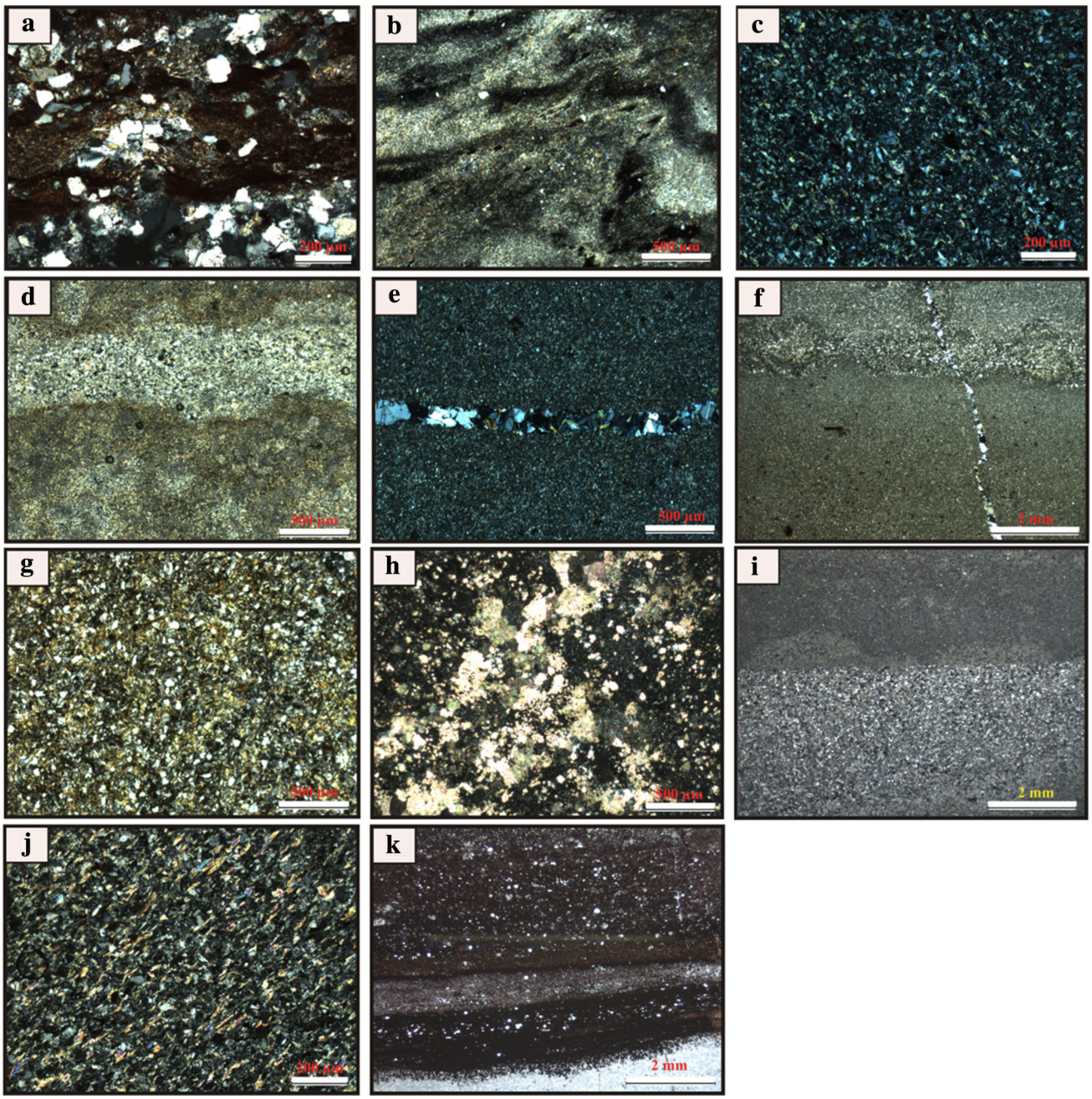

Fig. 3 Microscopical features of the Tadpatri shale samples those are used for geochemical analysis. **a** S-1 sample: dominated by clay materials with medium to coarse silt sized quartz grains; **b** S-2 sample: dominated by clay and ferruginous materials with fine silt sized quartz grains; **c** S-3 sample: dominated by clay minerals, micas, quartz grains with a very small proportion of plagioclase feldspar; **d** S-4 sample: relatively thin, wavy laminae of siltstone within shale showing distinct and sharp contact; **e** S-5 sample: micaceous to arenaceous shale with thin chert band, **f** S-6 sample: thick lamiane of siltstone within shale; **g** S-7 sample: dominated by ferruginous materials, micas and uniformly distributed quartz grains; **h** S-8 sample: dominated by carbonate cemented mud with sparry calcite; **i** S-9 sample: thick siltstone laminae within the shale showing sharp and straight boundary contact in between them; **j** S-10 sample: dominated by micas, quartz grains, ferruginous and clayey materials; mica minerals showing a preferred orientation; **k** S-11 sample: alternate band of siltstone, jasper and ferruginous shale with very less proportion of clayey materials

As the Tadpatri formation is unfossiliferous, its age is mainly reconstructed from the dating of intrusive sill and dykes. ^{40}Ar–^{39}Ar dating of phlogopite mica from Tadpatri formation indicates the initiation of volcanism at and around 1900 Ma (Anand et al. 2003). ^{206}Pb–^{204}Pb dating of Uranium mineralized strata reveals 1756 ± 29 Ma as a

Table 2 Major elements (in wt%) and trace elements (in ppm) concentrations in the Tadpatri shales with average composition of PAAS (Taylor and McLennan 1985)

Lithology	Shale											PAAS
Sample no.	S-1	S-2	S-3	S-4	S-5	S-6	S-7	S-8	S-9	S-10	S-11	
Major oxides												
SiO_2	68.65	55.19	58.83	59.71	61.12	61.99	60.18	52.83	64.04	61.91	80.32	62.80
TiO_2	0.42	0.65	0.57	0.60	0.59	0.61	0.61	0.36	0.52	0.49	0.17	0.99
Al_2O_3	15.35	21.87	20.14	19.43	16.46	18.56	19.08	9.37	16.58	18.86	2.50	18.90
Fe_2O_3	4.03	8.47	5.68	5.29	6.35	6.44	8.12	3.53	6.03	7.03	15.32	7.22
MnO	0.02	0.01	0.09	0.02	0.04	0.05	0.07	0.06	0.07	0.01	0.16	0.11
MgO	3.76	1.52	3.16	4.73	4.48	4.14	2.41	4.09	3.09	1.81	0.01	2.20
CaO	0.25	0.15	0.35	0.38	0.26	0.25	0.27	16.34	0.33	0.22	0.25	1.30
Na_2O	0.04	0.11	0.12	3.47	2.71	1.55	2.51	0.87	2.85	0.14	0.01	1.20
K_2O	3.97	8.10	7.80	2.53	1.64	2.50	2.45	1.23	1.77	3.61	0.16	3.70
P_2O_5	0.07	0.08	0.06	0.10	0.02	0.07	0.07	0.13	0.06	0.07	0.16	0.16
LOI	3.04	3.31	2.79	3.09	5.97	3.55	3.79	10.52	4.24	5.32	0.50	–
Trace elements												
Cs	2.10	8.19	5.65	0.91	3.78	2.83	2.98	1.16	3.70	3.36	1.21	15.00
Ba	1193.07	1230.51	3244.85	342.18	953.47	999.24	882.62	291.75	399.97	607.04	157.75	350.00
Pb	7.47	6.60	8.05	6.51	5.07	5.06	7.71	6.10	5.86	5.93	5.55	20.00
Rb	144.55	284.52	254.81	101.25	234.54	123.31	118.30	92.70	78.94	184.73	44.28	160.00
Sr	45.37	57.97	81.81	54.73	29.49	55.89	54.82	84.85	11.45	39.06	42.06	200.00
Ga	13.18	28.34	26.91	21.87	24.37	21.81	22.05	14.20	20.94	25.99	2.48	17.50
Cr	58.51	113.51	101.31	84.56	84.62	82.14	83.87	68.16	85.52	91.30	35.01	110.00
Ni	69.84	54.90	46.36	36.91	38.60	32.81	40.01	33.79	38.20	41.45	25.85	55.00
V	66.16	135.57	119.18	82.49	91.77	73.97	90.13	82.78	84.57	101.16	36.67	150.00
Sc	15.72	20.77	18.07	16.85	15.80	17.40	17.57	17.20	10.45	19.51	13.56	16.00
Co	20.69	17.10	22.72	14.70	12.70	19.91	24.01	10.68	17.45	18.00	11.06	23.00
Cu	34.32	33.46	88.29	43.92	40.11	30.67	37.28	33.15	34.92	32.76	33.71	50.00
Zn	90.91	100.15	45.55	75.77	46.73	54.18	192.04	63.17	51.36	42.72	77.75	85.00
Y	22.40	17.14	22.31	18.59	19.66	36.15	19.21	11.00	21.23	26.42	10.06	27.00
Zr	214.30	146.98	132.41	241.03	160.70	226.73	247.99	92.18	215.33	166.09	19.47	210.00
Hf	6.08	4.51	4.07	6.97	5.26	6.59	7.16	2.77	6.73	5.15	0.59	5.00
Nb	9.10	15.99	14.38	18.78	16.95	16.63	17.42	8.44	21.42	14.11	1.31	1.90
Th	14.83	16.03	18.29	15.46	22.55	19.85	21.07	9.48	13.45	19.14	1.87	14.60
U	2.89	2.98	3.08	3.26	3.93	4.15	3.53	2.37	1.70	2.64	0.72	3.10
Ta	0.94	1.50	1.33	1.59	1.79	1.48	1.45	0.80	1.95	1.22	0.12	–
CIA	77.61	70.55	69.5	68.1	71.07	76.55	72.47	69.08	69.77	81.19	92.38	70.38
CIW	99.15	98.37	98.08	75.33	76.97	86.17	80.59	76.6	75.89	97.62	98.7	82.72
PIA	98.82	97.31	96.73	72.4	74.88	84.18	78.14	73.74	73.57	97.01	98.61	79.05
ICV	0.81	0.87	0.88	0.87	0.97	0.83	0.86	2.82	0.88	0.71	6.37	0.88
K_2O/Al_2O_3	0.26	0.37	0.39	0.13	0.10	0.13	0.13	0.13	0.11	0.19	0.06	0.20
Al_2O_3/TiO_2	36.55	33.65	35.33	32.38	27.90	30.43	31.28	26.03	31.88	38.49	14.71	19.09
La/Sc	2.50	0.72	3.71	0.50	2.19	5.69	1.54	1.18	1.46	2.84	1.07	2.39
Th/Sc	0.94	0.77	1.01	0.92	1.43	1.14	1.20	0.55	1.29	0.98	0.14	0.91
Th/Co	0.72	0.94	0.80	1.05	1.77	1.00	0.88	0.89	0.77	1.06	0.17	0.63
Th/Cr	0.25	0.14	0.18	0.18	0.27	0.24	0.25	0.14	0.16	0.21	0.05	0.13
Zr/Hf	35.23	32.61	32.53	34.58	30.56	34.43	34.63	33.26	32.00	32.27	32.73	42.00
U/Th	0.19	0.19	0.17	0.21	0.17	0.21	0.17	0.25	0.13	0.14	0.39	0.21
Cu/Zn	0.38	0.33	1.94	0.58	0.86	0.57	0.19	0.52	0.68	0.77	0.43	0.59

Table 2 continued

Lithology	Shale											PAAS
Sample no.	S-1	S-2	S-3	S-4	S-5	S-6	S-7	S-8	S-9	S-10	S-11	
Ni/Co	3.37	3.21	2.04	2.51	3.04	1.65	1.67	0.11	2.19	2.30	2.34	2.39
V/Cr	1.13	1.19	1.18	0.98	1.08	0.90	1.07	1.21	0.99	1.11	1.05	1.36

minimum age for carbonate sedimentation (Zachariah et al. 1999). French et al. (2008) obtained 1885.4 ± 3.1 Ma for a gabbronorite sill body and considered this as the primitive depositional age of the Tadptari formation. K–Ar dating on arc-concentric mafic sills from the top portion of the Tadpatri formation indicates 958 ± 29 and 809 ± 29 Ma as the emplacement age of these sills (Murthy et al. 1987). Therefore, based on these previous radiometric datings we can determine that the Tadpatri formation may range between Late Palaeoproterozic to Mesoproterozoic age.

3 Materials and methods

Eleven shale samples (S1–S11; Fig. 2) were collected from different exposures located between the Sidhhanagar-II (N15°13′38.72″, E77°50′30.84″) and Nereducherla areas (N15°12′12.17″, E77°53′42.89″), in the northwestern portion of the Cuddapah basin (Fig. 1c). To remove contamination, all the samples were cleaned with distilled water. This was followed by subsequent air drying, powdering in a mortar, and finally sieving through a 200 ASTM mesh.

Major element concentrations were obtained by a Bruker model S4 Pioneer sequential wavelength—dispersive X-ray fluorescence (XRF) spectrometer, and the trace and rare earth elements were analyzed by high resolution inductively coupled plasma mass spectrometer (HR-ICP-MS) in which GSR-5 was used as the standard. At first, 50 mg of each sample was taken in Savillex vessels and 10 mL of 7:3 HF–HNO_3 acid mixture was added to that sample. The vessels were then tightened and placed on the hot plate at 150 °C for 50 h. After that, the vessels were opened and a single drop of $HClO_4$ was added to the mixtures, which were further evaporated to near dryness at 160 °C. The rest of the residues of each vessel were dissolved by adding 20 mL of 1:1 HNO_3–Milli-Q water and placing them on the hot plate for 30–45 min at 100 °C in order to dissolve all suspended particles. Subsequently, Rhodium solution (in an amount 5 mL) was added as an internal standard to each vessel, and the volume was raised to 250 mL by adding Milli-Q water. This solution of each sample was stored in High Density Polyethylene (HDPE) bottles. 5 mL of this solution was mixed again with 50 mL Milli-Q water (1:10 ratio) and stored in Eppendorf tubes for analysis. The analytical precision of the geochemical data is better than 5% RSD.

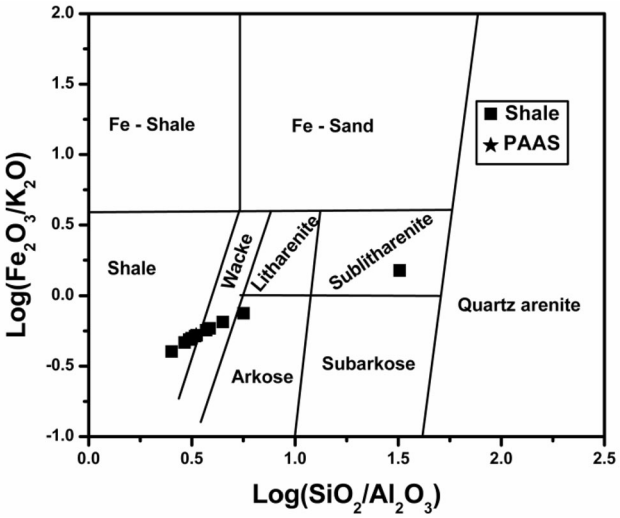

Fig. 4 Geochemical classification of Tadpatri shales using the major element composition (Reproduced with permission from Herron 1988)

4 Results

4.1 Petrography

The studied section of the Tadpatri formation is dominated by shale with minor amounts of carbonates and sill bodies (Fig. 2). The shales recorded in this section are of different varieties In the basal part, the shale (Sample S-1) is interbedded with a thin band of sandstone. Microscopically this shale (Sample S-1) is dominated by clay minerals and quartz with relatively smaller amounts of ferruginous materials and micas (Fig. 3a). This shale type is followed by the dark grey shale with distorted ferruginous laminae (Sample S-2). Under the microscope, sample S-2 is dominated by clay minerals, ferruginous materials and micas with a smaller proportion of quartz when compared to Sample S-1 (Fig. 3b). The red to dark grey colored ferruginous laminae are moderately to highly distorted. Sample S-3 is massive grey-greenish shale, dominated by clay minerals, muscovite, biotite, quartz and ferruginous

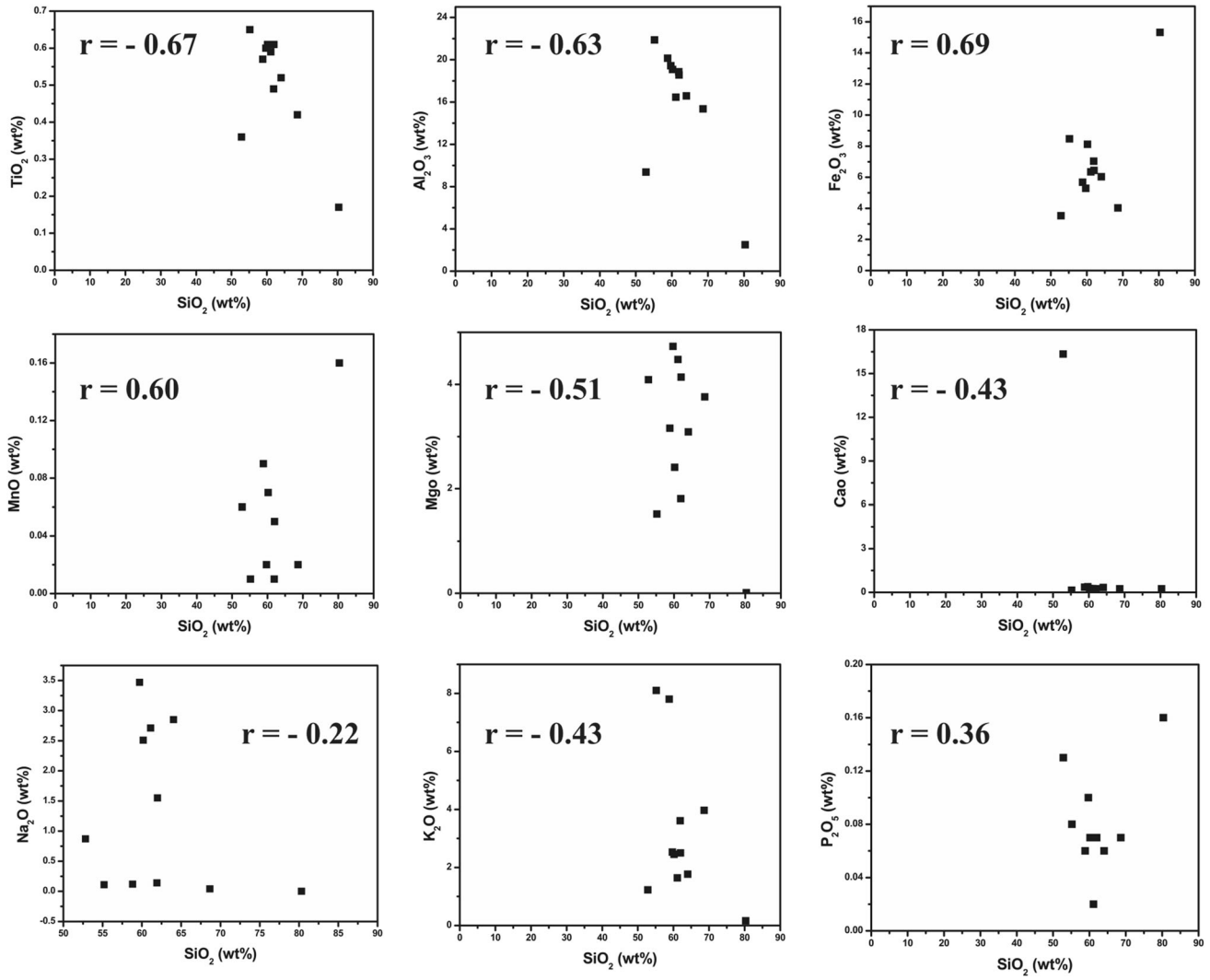

Fig. 5 Binary plots of the Tadpatri shales against SiO_2

materials (Fig. 3c). A very small proportion of plagioclase feldspar is also present in sample S-3, but not very persistent throughout all the microscopic studies. Sample S-4 is grey colored laminated shale, dominated by micaceous shale with distinctive thin laminated siltstone (Fig. 3d). The contact between the siltstone laminae and shale is sharp and wavy in nature. Individual grains within siltstone laminations are very fine to medium silt sized, subrounded to subangular shaped and moderate to well sorted. Sample S-5 is laminated shale with occasional development of chert band (Fig. 3e). Sample S-6 also represents the dark grey colored laminated shale but differs from sample S-4. Sample S-6 is dominated by micaceous to arenaceous shale with relatively thick siltstone laminae (Fig. 3f). The contact between the siltstone laminae and shale is sharp and wavy. Individual grains within the siltstone laminations are fine silt sized, subrounded to subangular shaped. Sample S-7 represents the reddish brown ferruginous shale, which is microscopically dominated by clay minerals, ferruginous material, mica minerals and quartz (Fig. 3g). The quartz grains are nearly distributed in a uniform way, fine to medium silt sized and rounded to subrounded in shape. Sample S-8 is calcareous shale and found in an association with carbonates. This calcareous shale is dominated by massive, dark grey to black carbonate cemented mud with sparry calcite (Fig. 3h). Minor amounts of terrigenous silt are also present. Sample S-9 represents the dark grey laminated shale from the upper part of the studied section. The siltstone laminae are relatively thick and the contact between the siltstone laminae and shale is sharp and straight (Fig. 3i). Sample S-10 represents massive dark grey shale, dominated by clay minerals, muscovite, biotite and fine quartz grains (Fig. 3j). The mica minerals are showing a preferred orientation. Sample S-11 is the reddish brown ferruginous shale with distinct chert and jasper band and dominate the upper most part of the studied

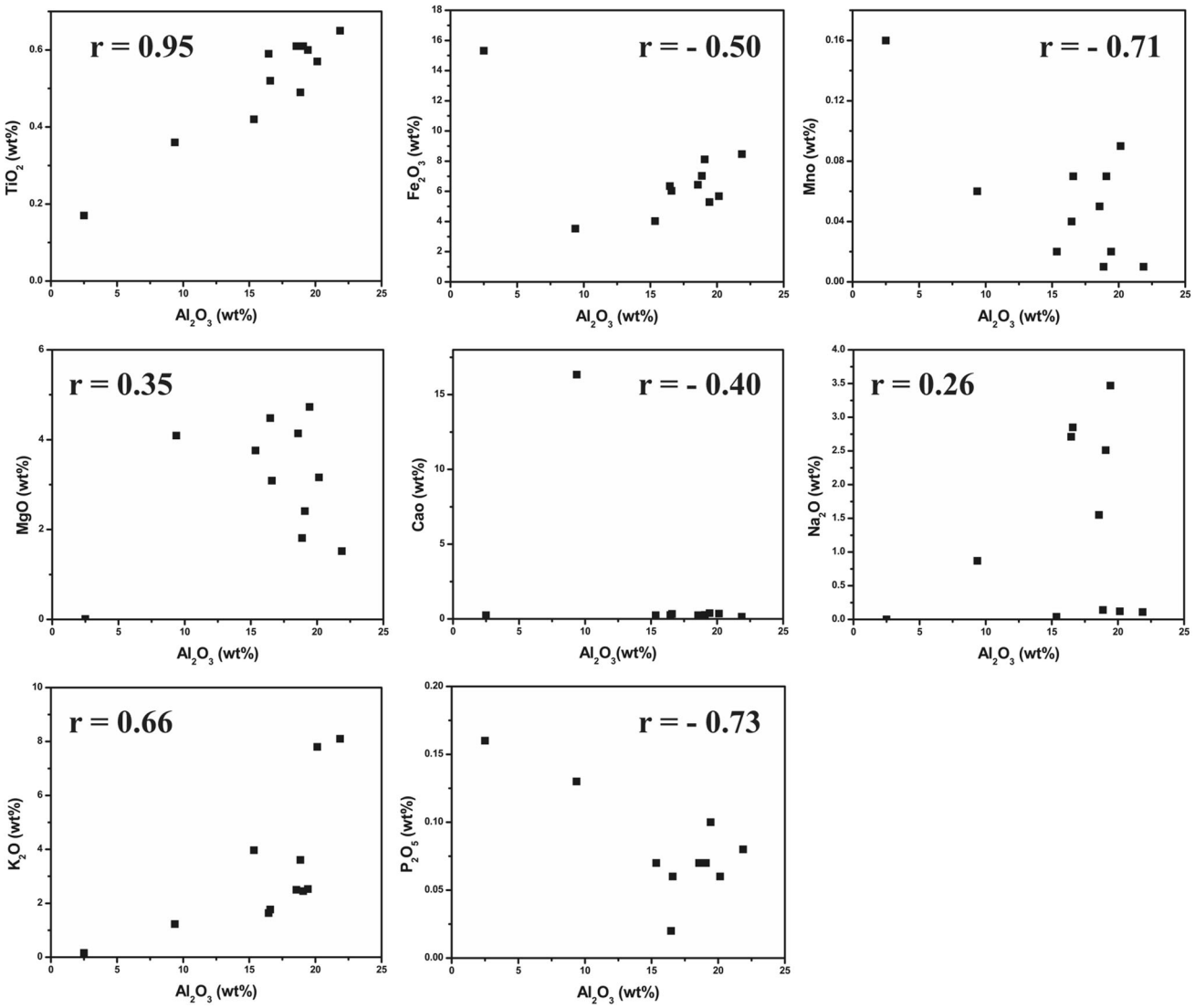

Fig. 6 Binary plots of the Tadpatri shales against Al_2O_3

section. Under microscopic study, alternate banding of siltstone, jasper, and ferruginous shale is prominent with variable thickness (Fig. 3k).

4.2 Major elements

Table 2 represents the major oxides data of the shale samples (n = 11). Tadpatri shales (except S-8 and S-11) from the study area fall in the field of shale and wacke of the bivariate plot, log (SiO_2/Al_2O_3) versus log (Fe_2O_3/K_2O) (Fig. 4; Herron 1988). S-6 sample is overlapped with the average PAAS value (Taylor and McLennan 1985) in this diagram. In comparison with average PAAS value most of the shale samples (except S-8 and S-11) are showing similar SiO_2, Al_2O_3 wt%. In contrast, the S-11 sample is depleted in MgO, CaO, K_2O and Na_2O, which indicates an extreme weathering of the source area or preferably several recycling processes (Chakrabarti et al. 2009). Also high weight percentage of Fe_2O_3 in S-11 indicates greater availability of iron compounds in seawater, which is co-sedimented during the rock unit accumulation. This may result from mafic volcanism prior to sedimentation of this shale horizon (Pettijhon 1975).

Bivariate plots of SiO_2 versus TiO_2, Al_2O_3, MgO, CaO and K_2O of the Tadpatri shales exhibit negative correlation ($0 > r \geq -1$, $n = 11$) whereas SiO_2 versus Fe_2O_3, MnO, and P_2O_5 of these samples display positive correlation ($0 < r \leq 1$, $n = 11$) (Fig. 5). However, TiO_2, MgO and K_2O display positive correlation ($0 < r \leq 1$, $n = 11$) with Al_2O_3 (Fig. 6). This implies that the distribution of K_2O, TiO_2 and MgO within the rock is possibly controlled by Al_2O_3. SiO_2 versus Na_2O bivariate plot reflects two trends

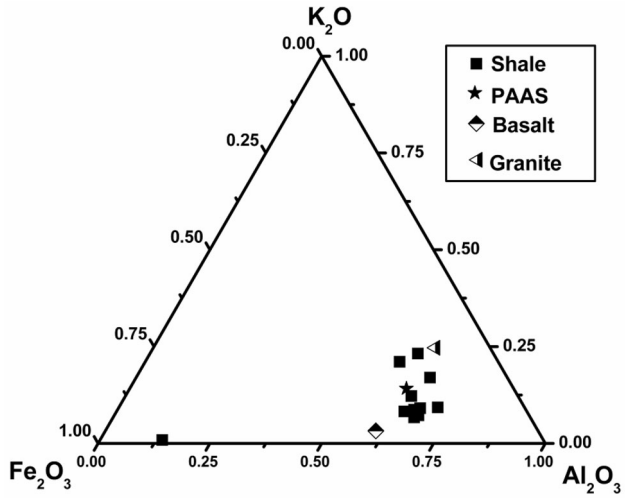

Fig. 7 Major element distribution in the Tadpatri shales in Fe_2O_3–K_2O–Al_2O_3 compositional space. The data on granite, basalt and PAAS are defined from Condie (1993) and Taylor and McLennan (1985) respectively

(horizontal and positive) (Fig. 5) between Si–Na. A similar consideration is also observed between Al–Na (Al_2O_3 versus Na_2O plot; Fig. 6).

The ternary diagram of Fe_2O_3–K_2O–Al_2O_3 (Fig. 7) shows that most of the shale samples (except S-11) are plotted near Al_2O_3 apex. This indicates their enrichment in Al_2O_3, which further implies that the element abundances are predominantly controlled by clay minerals (Wronkiewicz and Condie 1987). The K_2O/Al_2O_3 ratio of sediment is used as the index of initial composition of ancient sediments; for example, for clay minerals and feldspars it is 0.0–0.3 and 0.3–0.9, respectively (Cox et al. 1995). For the Tadpatri shale samples the K_2O/Al_2O_3 ratio shows a variation from 0.06 to 0.39 with an average of 0.18 (Table 2). As the K_2O/Al_2O_3 ratio in some shale samples is near the upper limit of clay mineral, illite is considered to be the dominant clay mineral (Chakrabarti et al. 2009).

4.3 Trace elements

Table 2 also represents the trace elements data with the elemental ratios of the shale samples. PAAS normalized trace elements are plotted in a multielement diagram, which shows depletion of Cs, Pb, Sr, Cr, Ni, V, Co and moderate to slight enrichment of Nb, Th, and U (Fig. 8a).

Within high field strength elements (HFSE) the element pairs Hf–Zr and Ta–Na are very much identical in size and charge; therefore they show similar geochemical behavior. In the Tadpatri shale samples, Zr has a very strong correlation ($r = 0.99$, $n = 11$) with Hf, while Nb has a very strong correlation ($r = 0.98$, $n = 11$) with Ta (Table 3). This indicates their similarity in geochemical behavior and also implies that they are not differentiated during the weathering process (Long et al. 2012; Armstrong-Altrin et al. 2017). All the HFSEs of the Tadpatri shales show good positive correlations between them and also have a positive correlation with TiO_2 (Table 3).

Sr values within the shale samples vary from 11.45 to 84.85 ppm with an average 50.68 ppm. Sr has no effective positive correlation with Al_2O_3 and K_2O, whereas it is positively correlated (moderate, $r = 0.54$, $n = 11$; Table 3) with CaO, indicating their affinity to Ca. The concentration of Ba ranges between 157.75 and 3244.85 ppm, which is positively correlated with K_2O ($r = 0.78$, $n = 11$; Table 3). This barium concentration can be treated as a proxy of detrital flux. Tadpatri shale samples are showing overall enrichment in Barium, and this is may be due to their deposition in a shallow marine condition (Nagarajan et al. 2007). Within these trace elements, Cs, Rb, Cr, V, Sc, and Co are showing positive correlation with Al_2O_3 and K_2O (Table 3). This implies that these elements are mainly concentrated within the clay mineral and are accumulated during weathering process (Fedo et al. 1996; Armstrong-Altrin et al. 2015a, b).

4.4 Rare earth elements

Table 4 represents the rare earth elements (REE) data of the shale samples. The concentration of $\sum$REE within the Tadpatri shales varies from 51.56 to 406.92 ppm. The bulk REE are generally bounded within the fine clastic with the understanding that trivalent REE are easily settled in clay mineral, which is typically enriched in alumina and ferric iron (Nagarajan et al. 2007; Ramos-Vázquez et al. 2017). The chondrite normalized REE plot (Fig. 8b) of this Tadpatri shale show moderately inclined LREE (La–Eu section) and nearly flat HREE (Gd–Lu section) patterns with negative Eu anomaly (Fig. 8b). Eu/Eu* values of all the Tadpatri shale samples are within 0.50 and 0.80 (< 0.85, Table 4), which indicate their recycling from upper continental crust (UCC). The negative Eu anomaly with 1.54 average value of Gd_n/Yb_n ratio is also a distinctive feature of Tadpatri shales, which indicates their deposition in Post Archean timescale (Taylor and McLennan 1985).

5 Discussion

5.1 Paleoweathering

Numerous geochemical parameters are frequently used to determine the weathering intensity of source rock. Within these parameters, the Chemical Index of Alteration (CIA) and A–CN–K diagram are the most important

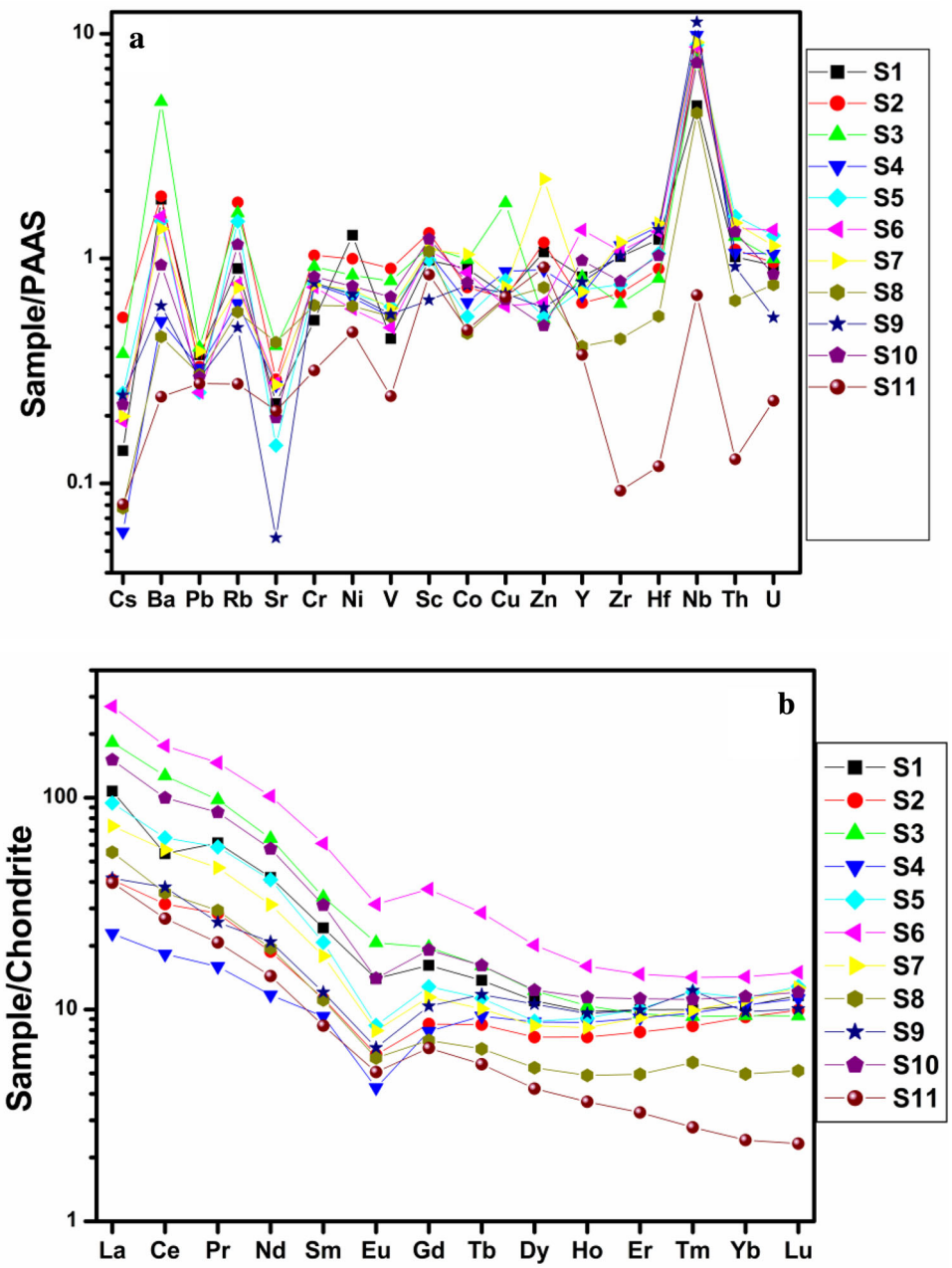

Fig. 8 Distribution of **a** PAAS-normalized trace elements and **b** Chondrite normalized REE elements in Tadpatri shales. PAAS and Chondrite normalized values are defined from Taylor and McLennan (1985)

(Manikyamba et al. 2008; Nagarajan et al. 2014). CIA is considered as the ratio of primary mineral and clay mineral and is formulated as $[Al_2O_3/(Al_2O_3 + CaO^* + K_2O + Na_2O)] \times 100$ (Nesbitt and Young 1982, 1984). The value is expressed in molar proportion, and CaO* represents CaO present in silicate mineral, following McLennan (1993). In unweathered igneous rock the CIA value is around 50, and for intensely weathered rock (mainly composed of kaolinite, gibbsite), the value is near 100 (Nesbitt and Young 1984). The CIA computed for Tadpatri shale samples have values ranging from 68.10 to 92.38 with an average 74.39 (Table 2), which is comparatively high and indicates high weathering of the source rock. A comparative study of CIA between shale samples and PAAS shows more or less a similar weathering intensity of the source rocks (Fig. 2). The K_2O/Al_2O_3 ratio (average 0.18) of the Tadpatri shales indicates the presence of illite clay, which further suggests that the sediment is mainly derived in a cold climatic condition (Chakrabarti et al. 2009). In $Al_2O_3 - (Cao^* + Na_2O) - K_2O$ (A–CN–K) diagram (Fig. 9) the direction of ideal weathering is parallel to A–CN side, and as the weathering continues, the direction advanced near to the illite composition (Fedo et al. 1995). In this diagram, some Tadpatri shales are plotted close to the Al_2O_3–K_2O line, which indicates intense weathering of the source rock (Hessler and Lowe

Table 3 Correlation matrix between major and trace elements in the Tadpatri shales

	Cs	Ba	Pb	Rb	Sr	Cr	Ni	V	Sc	Co	Y	Zr	Hf	Nb	Ta	Th	U
SiO_2	− 0.39	− 0.25	− 0.20	− 0.48	− 0.47	− 0.76	− 0.14	− 0.77	− 0.56	− 0.15	− 0.13	− 0.33	− 0.35	− 0.56	− 0.56	− 0.54	− 0.58
TiO_2	0.56	0.38	0.18	0.58	0.02	0.87	0.26	0.73	0.43	0.53	0.54	0.73	0.76	0.89	0.88	0.87	0.81
Al_2O_3	0.60	0.47	0.34	0.64	0.03	0.89	0.44	0.67	0.50	0.66	0.60	0.73	0.76	0.83	0.80	0.85	0.72
MgO	− 0.24	0.10	− 0.04	0.04	0.14	0.20	0.11	0.08	− 0.03	0.03	0.34	0.55	0.56	0.48	0.53	0.48	0.65
CaO	− 0.33	− 0.25	− 0.08	− 0.25	0.54	− 0.20	− 0.22	− 0.06	0.06	− 0.48	− 0.44	− 0.36	− 0.38	− 0.32	− 0.31	− 0.35	− 0.16
Na_2O	− 0.27	− 0.34	− 0.21	− 0.28	− 0.37	0.15	− 0.35	− 0.07	− 0.37	− 0.06	0.09	0.60	0.63	0.69	0.66	0.35	0.34
K_2O	0.83	0.78	0.58	0.82	0.39	0.72	0.63	0.82	0.62	0.53	0.21	0.09	0.10	0.24	0.25	0.36	0.29
P_2O_5	− 0.48	− 0.44	− 0.07	− 0.61	0.33	− 0.62	− 0.39	− 0.52	− 0.10	− 0.50	− 0.59	− 0.60	− 0.67	− 0.72	− 0.81	− 0.89	− 0.68
U	0.23	0.37	0.09	0.50	0.22	0.55	0.23	0.43	0.52	0.44	0.61	0.64	0.64	0.57	0.60	0.88	
Th	0.40	0.42	0.15	0.59	− 0.04	0.70	0.29	0.58	0.43	0.59	0.66	0.70	0.74	0.74	0.76		
Ta	0.42	0.18	− 0.02	0.39	− 0.32	0.76	0.13	0.57	0.01	0.35	0.48	0.73	0.80	0.98			
Nb	0.37	0.14	0.03	0.29	− 0.28	0.76	0.07	0.55	0.05	0.41	0.50	0.78	0.84				
Hf	0.06	0.04	0.17	0.08	− 0.30	0.47	0.30	0.25	0.02	0.59	0.62	0.99					
Zr	0.01	0.03	0.22	0.03	− 0.24	0.41	0.32	0.20	0.04	0.61	0.62						
Y	0.17	0.29	− 0.12	0.21	− 0.15	0.37	0.15	0.16	0.19	0.59							
Co	0.37	0.61	0.66	0.29	0.10	0.43	0.48	0.36	0.25								
Sc	0.43	0.36	0.28	0.65	0.61	0.54	0.28	0.63									
V	0.84	0.56	0.35	0.84	0.27	0.95	0.37										
Ni	0.41	0.43	0.58	0.51	0.04	0.26											
Cr	0.78	0.48	0.23	0.75	0.14												
Sr	0.04	0.44	0.45	0.20													
Rb	0.84	0.69	0.25														
Pb	0.23	0.59															
Ba	0.59																

Table 4 REE (in ppm) concentrations in the Tadpatri shales with average composition of PAAS (Taylor and McLennan 1985)

Lithology	Shale											PAAS
Sample no.	S-1	S-2	S-3	S-4	S-5	S-6	S-7	S-8	S-9	S-10	S-11	
La	39.38	15.04	66.96	8.39	34.65	99.05	27.00	90.13	15.28	55.40	14.57	38.20
Ce	52.12	30.16	121.44	17.48	61.90	168.37	54.29	34.04	36.15	95.50	25.74	79.60
Pr	8.38	3.89	13.40	2.19	8.02	20.06	6.40	4.02	3.53	11.70	2.84	8.83
Nd	29.89	13.34	45.68	8.32	29.17	72.35	22.26	13.87	14.85	40.78	10.24	33.90
Sm	5.61	2.60	7.84	2.14	4.80	14.07	4.14	2.56	2.79	7.19	1.94	5.55
Eu	1.22	0.53	1.80	0.37	0.73	2.73	0.69	0.51	0.57	1.22	0.44	1.08
Gd	4.94	2.61	6.01	2.41	3.92	11.32	3.49	2.19	3.17	5.84	2.01	4.66
Tb	0.80	0.49	0.93	0.54	0.66	1.66	0.58	0.38	0.68	0.94	0.32	0.77
Dy	4.19	2.82	4.66	3.33	3.36	7.68	3.20	2.02	4.04	4.70	1.61	4.68
Ho	0.83	0.63	0.88	0.74	0.77	1.36	0.70	0.42	0.81	0.97	0.31	0.99
Er	2.48	1.95	2.37	2.27	2.51	3.66	2.28	1.23	2.47	2.80	0.81	2.85
Tm	0.36	0.30	0.33	0.34	0.43	0.50	0.35	0.20	0.44	0.40	0.10	0.41
Yb	2.58	2.28	2.32	2.60	2.82	3.54	2.74	1.23	2.42	2.85	0.60	2.82
Lu	0.44	0.38	0.36	0.43	0.49	0.57	0.48	0.20	0.38	0.46	0.09	0.43
$\sum$ LREE/$\sum$ HREE	8.22	5.72	14.39	3.07	9.31	12.43	8.30	9.58	5.08	11.17	9.53	9.43
$\sum$ REE	153.22	77.02	274.99	51.56	154.22	406.92	128.60	83.17	87.59	230.75	61.62	184.77
Eu/Eu*	0.71	0.63	0.80	0.50	0.52	0.66	0.56	0.66	0.59	0.57	0.68	0.65
(Gd_n/Yb_n)	1.55	0.93	2.10	0.75	1.13	2.59	1.03	1.44	1.06	1.66	2.72	1.34

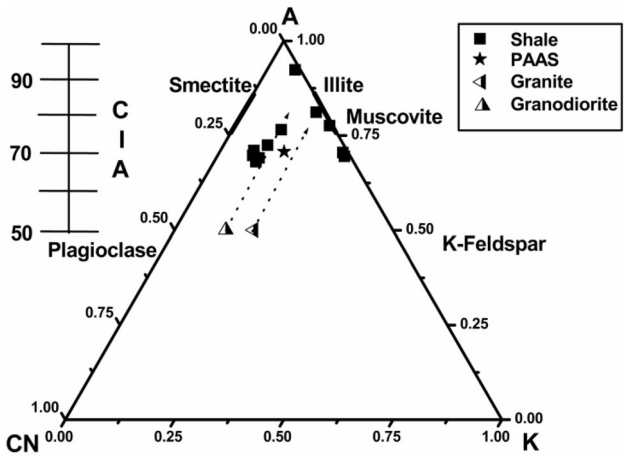

Fig. 9 Molecular proportions of A-CN-K diagram for the shales of Tadpatri formation, after Nesbitt and Young (1984). The dashed arrows represent weathering trend of Granite and Granodiorite (Reproduced with permission from Nesbitt and Young 1984)

2006). The CIA value may be decreased due to K-metasomatism and therefore the Plagioclase Index of Alteration (PIA) and Chemical Index of Weathering (CIW) values are considered to better estimate the weathering of source rock. PIA and CIW are formulated as $[(Al_2O_3 - K_2O)/(Al_2O_3 + CaO^* - K_2O + Na_2O)] \times 100$ and $[Al_2O_3/(Al_2O_3 + CaO^* + Na_2O)] \times 100$, respectively (Fedo et al. 1995; Harnois 1988). Higher average values of PIA and CIW (85.94 and 87.59 respectively, Table 2) of Tadpatri shales also indicate that the source rock has suffered intense weathering.

The Index of Compositional variability (ICV) also indicates the original composition of fine clastic rock and is formulated as $(Fe_2O_3 + K_2O + Na_2O + CaO + MgO + TiO_2)/Al_2O_3$. Compared to the clay minerals, non-clayey minerals (pyroxene, feldspar) show higher ICV values (> 1) (Cullers and Podkovyrov 2000). Therefore, shale with high ICV values indicates the presence of higher amounts of non-clayey minerals and is considered to be immature (Cox et al. 1995). All of the Tadpatri shales except S-8 and S-11 have ICV value less than 1 and therefore are considered to be mature (Table 2). Sample S-8 and S-11 have ICV values that are greater than 1 mainly due to their enrichment in carbonate (CaO) and ferruginous (Fe_2O_3) component, respectively.

5.2 Provenance

The geochemical characteristics of shale have been widely used to depict the provenance nature (Cullers 2000; Armstrong-Altrin et al. 2004; Sun et al. 2013). Al_2O_3/TiO_2 ratio distinctly varies from mafic (3–8) to intermediate (8–21) as well as in felsic rocks (21–70) (Hayashi et al. 1997). Therefore Al_2O_3/TiO_2 ratio of the sediments, derived from those igneous rocks can be used as a proxy of source rock composition (Armstrong-Altrin 2009). In Tadpatri shale

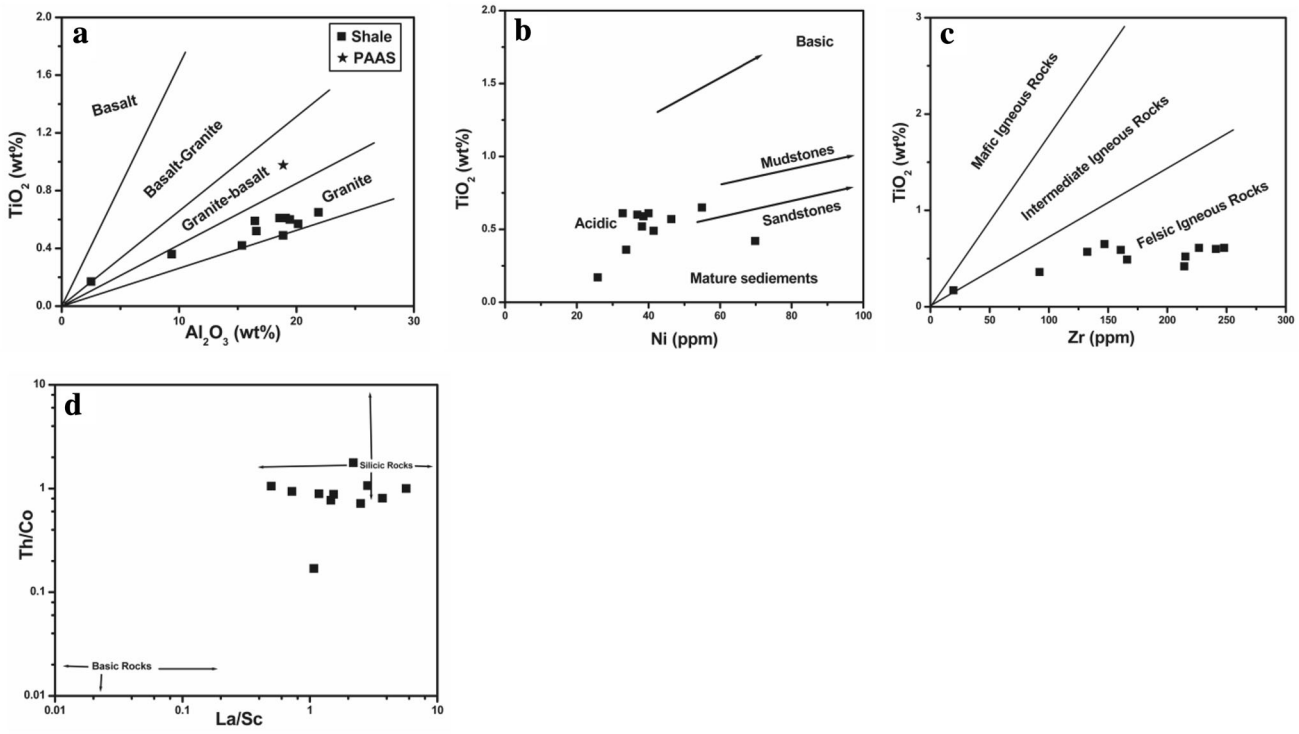

Fig. 10 Scatter plots of **a** Al_2O_3 versus TiO_2; **b** Ni versus TiO_2; **c** Zr versus TiO_2 and **d** La/Sc versus Th/Co indicate the derivation of Tadpatri shales from felsic source rocks

Table 5 Range of elemental ratios of Tadpatri shales compared to the ratios derived from felsic rocks (Cullers 2000), mafic rocks (Cullers 2000), upper continental crust (Taylor and McLennan 1985) and PAAS (Taylor and McLennan 1985)

Elemental ratio	Ranges of sediments		Upper continental crust	PAAS	Ranges of shale from Tadpatri formation		Average value
	Felsic rocks	Mafic rocks			S-1,S-2,S-3,S-4,S-5,S-6,S-7,S-8,S-9, S-10	S-11	Tadpatri shales
Th/Sc	0.84–20.5	0.05–0.22	0.97	0.91	0.55–1.43	0.14	0.94
Th/Co	0.67–19.4	0.04–1.40	1.07	0.63	0.72–1.77	0.16	0.91
Th/Cr	0.13–2.7	0.018–0.046	0.30	0.13	0.14–0.27	0.05	0.19
La/Co	1.80–13.80	0.14–0.38	3.00	1.66	0.57–4.97	1.32	2.03
La/Sc	2.50–16.3	0.43–0.86	2.72	2.39	0.50–5.69	1.07	2.13

samples, Al_2O_3/TiO_2 varies between 26.03 and 38.49 (excluding S-11 sample with 14.70 Al_2O_3/TiO_2) with the average of 30.78 (Table 2). This suggests that felsic granitoid to granite rocks are the probable source rocks. A comparative study of Al_2O_3/TiO_2 between Tadpatri shales and PAAS shows that Tadpatri shales derived from a more felsic source rock (Fig. 2). Plotting of the Tadpatri shale samples in the binary diagram Al_2O_3 versus TiO_2 (Amajor 1987) (Fig. 10a) demonstrates that except for S-11, all the shales are in the field of granite, which indicates their derivation from a felsic source rock. Ni versus TiO_2 bivariate plot (Fig. 10b; Floyd et al. 1989), Zr versus TiO_2 bivariate plot (Fig. 10c; Hayashi et al. 1997) and La/Sc versus Th/Co plot (Fig. 10d; Cullers 2002) also demonstrates the derivation of Tadpatri shales from a felsic rock.

Table 5 represents a range of trace element ratios (Th/Sc, Th/Co, Th/Cr, La/Co, La/Sc) of the Tadpatri shales. Trace elemental ratios of the clastics derived from felsic and mafic rocks are also given in Table 5, which shows a distinct separation in their ranges (Cullers 2000). Comparison of these elemental ratios with the Tadpatri shales' elemental ratio clearly demonstrates that the Tadpatri sediments derived from felsic rock.

Not only major and trace elements, but also REE with Eu anomaly plays a key role in depicting the source rock characteristic (Tapia-Fernandez et al. 2017). Higher LREE/

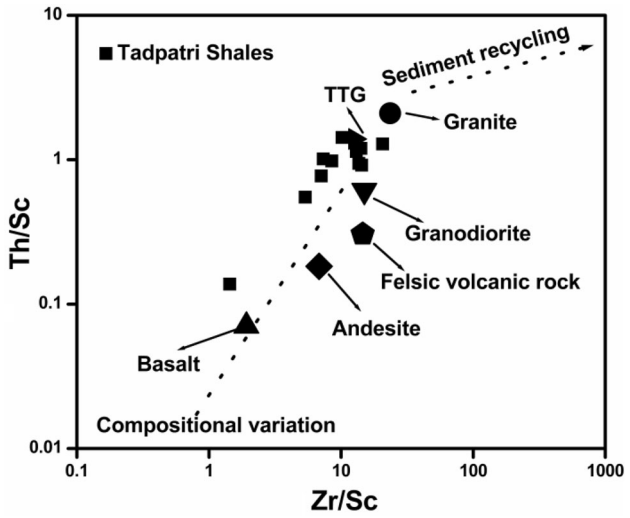

Fig. 11 Plot of Zr/Sc versus Th/Sc (after McLennan et al. 1993) regarding sedimentary sorting and provenance. The data on average rock compositions (granite, TTG, granodiorite, felsic volcanic rock, andesite, basalt) are defined from Condie (1993)

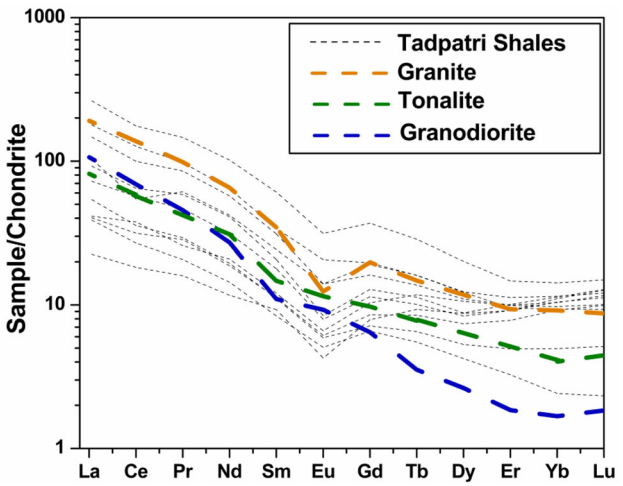

Fig. 12 Chondrite-normalized REE patterns of three potential source rocks (granite, tonalite, granodiorite) of Eastern Dharwar Craton with the Tadpatri shales

HREE ratio with a negative Eu anomaly indicates derivation from felsic rock and the lower LREE/HREE with no or a small Eu anomaly implies derivation from mafic rock (Cullers 1995). As the Tadpatri shales show high LREE/HREE ratios (average 8.80) (Table 4) with negative Eu anomaly, they also indicate their derivation from felsic source rock.

As Zr, Th, Sc are immobile and insoluble in nature, the plotting of Zr/Sc versus Th/Sc (Fig. 11) is applied to determine the sorting of zircon (McLennan et al. 1993; Spalletti et al. 2008). Tadpatri shale samples from this study area show a positive slope in the diagram. Most of the Tadpatri shales exhibit Zr/Sc and Th/Sc values near 10 and 1, respectively. According to this diagram, the zircon in the most shale samples is not winnowed during the sedimentary process. This observation is also supported by the average Zr/Hf ratio of the shale samples (33.17; Table 2), which is very much similar to the Zr/Hf ratio (33, Taylor and McLennan 1985) of UCC. A felsic source rock for the Tadpatri shales is also supported by this Zr/Sc versus Th/Sc diagram (Fig. 11) as most of the shales are well plotted within the field of granodiorite–TTG–granite.

As the lower Cuddapah Group of rocks developed over the Eastern Dharwar Craton, granite, granodiorite and tonalite of the Eastern Dharwar Craton are likely to be considered as the source rocks of the Tadpatri shales. For the source rock compilation we are following the methodology used in Armstrong-Altrin (2009). Based on that, the chondrite-normalized REE pattern of the Tadpatri shales is compared with the chondrite-normalized REE pattern of granite, granodiorite (Jayananda et al. 2000) and tonalite (Allen 1985) of the Eastern Dharwar Craton (Fig. 12) which clearly shows the derivation of the Tadpatri shales from a mixing of source rocks like granite, granodiorite, tonalite. The Eu/Eu* ratio of most of the shales is within the range of Tonalite (Eu/Eu* = 0.96, Allen 1985) and Granite (Eu/Eu* = 0.48, Jayananda et al. 2000). Therefore it can be presumed that granite and tonalite are the most dominant source rocks of the Tadpatri shales. This comparative chondrite-normalized REE diagram (Fig. 12) distinctly suggests that seven numbers of Tadpatri shales follow the trend of granite, 3 numbers of Tadpatri shales follow the trend of tonalite and a single sample follows the trend of granodiorite. Therefore we can argue that the Tadpatri shales are most likely derived from a felsic rock, which is a mixing of granite (65%), tonalite (25%) and granodiorite (10%) from the Eastern Dharwar Craton.

Major oxides data are applied for tectonic discrimination based plots (Bhatia 1983; Roser and Korsch 1986; Verma and Armstrong-Altrin 2013; Armstorng-Altrin 2015). Here we are considering the new discrimination diagrams proposed by Verma and Armstrong-Altrin (2013); Armstorng-Altrin (2015) as the success rate of these diagrams are relatively higher (75%–100% success rate) compared to the old discrimination diagrams proposed by Bhatia (1983) and Roser and Korsch (1986). The new tectonic diagrams (Verma and Armstrong-Altrin 2013) are applied to discriminate three major tectonic settings—arc, rift, and collision settings. Based on these diagrams the Tadpatri shales are grouped into high silica ($SiO_{2\ (adj)} > 63\% - \leq 95\%$; sample S-1, S-5, S-6, S-9, S-10, S-11) and low silica ($SiO_{2\ (adj)} > 35\% - \leq 63\%$; sample S-2, S-3, S-4, S-7, S-8) rocks and most of them (except sample S-11) are well plotted within arc and collision fields (Fig. 13a, b). There is an indiscrimination in the use of the discrimination

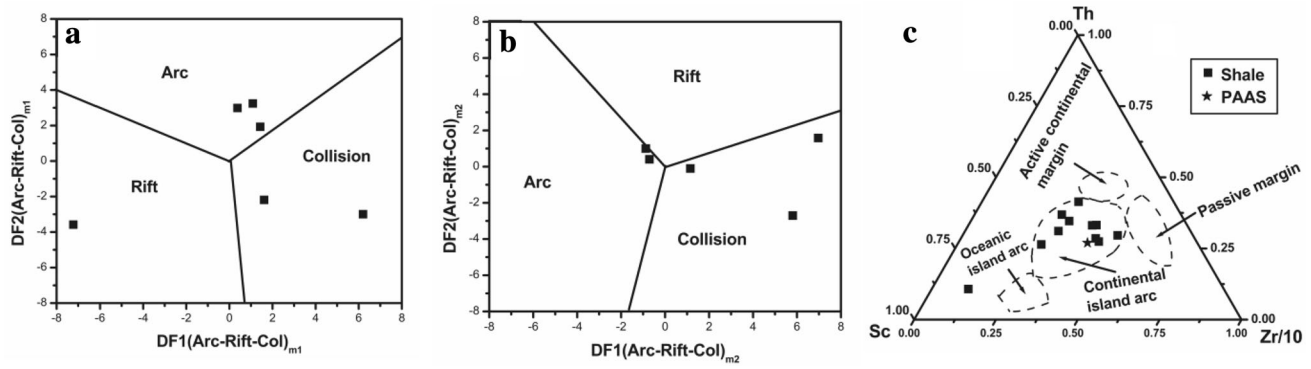

Fig. 13 Tectonic discrimination diagrams for Tadpatri shales **a** Fields are demarcated after Verma and Armstrong-Altrin (2013), the subscript m1 in DF1 and DF2 represents the high silica ($SiO_{2\ (adj)} > 63\% - \leq 95\%$) diagram based on $\log_e$ ratios of major elements, $SiO_{2\ (adj)}$ is the SiO_2 value calculated after volatile free adjustment of the ten major elements to 100 wt%, $SiO_{2\ (adj)}$ value of sample S-1, S-5, S-6, S-9, S-10, S-11 is 71.10, 65.25, 64.47, 67.17, 65.76, 81.08 respectively; **b** Fields are demarcated after Verma and Armstrong-Altrin (2013), the subscript m2 in DF1 and DF2 represents the low silica ($SiO_{2\ (adj)} > 35\% - \leq 63\%$) diagram based on $\log_e$ ratios of major elements, $SiO_{2\ (adj)}$ value of sample S-2, S-3, S-4, S-7, S-8 is 57.40, 60.77, 62.03, 62.84, 59.49 respectively; **c** Th–Sc–Zr/10 fields are demarcated after Bhatia and Crook (1986)

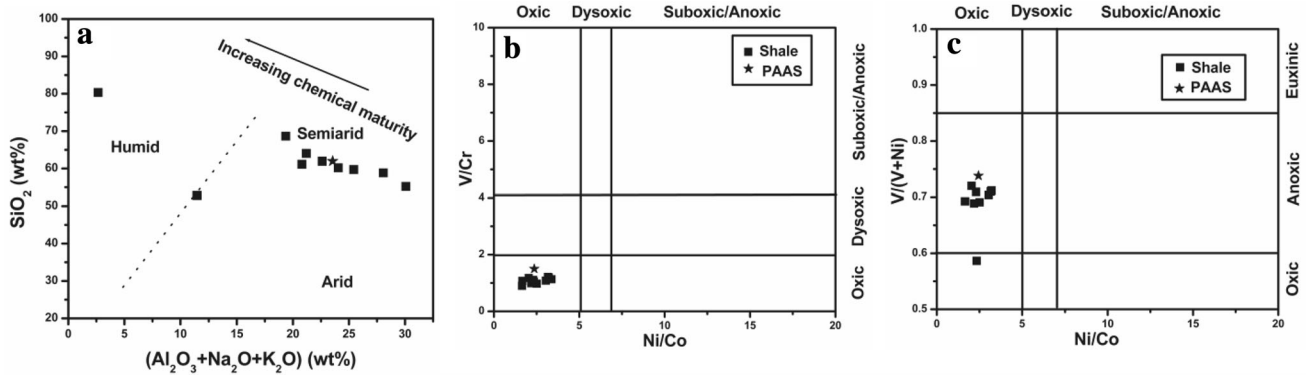

Fig. 14 Paleoenvironment of Tadpatri shales. **a** Binary plot of SiO_2 versus ($Al_2O_3 + Na_2O + K_2O$) indicates deposition is in mainly semiarid climate; **b** Binary plot of Ni/Co versus V/Cr indicates oxic condition during deposition and **c** Binary plot of Ni/Co versus V/(V + Ni) indicates oxic to anoxic condition during deposition

diagram, exclusively in which major oxides data are used for provenance study (Armstrong-Altrin and Verma 2005; Verma and Armstrong-Altrin 2013, 2016). In this respect, immobile trace elements (La, Th, Sc, Zr) are more reliably applied to study the tectonic setting (Mir 2015; Li et al. 2017). Ternary diagrams (Bhatia and Crook 1986) applied for tectonic discrimination also have some issues. In the La–Th–Sc ternary plot, the active and passive margins are marked by a single compositional field, and the success rate lies between 0% and 0.6% (Verma and Armstrong-Altrin 2016). Here we are considering only the Th–Sc–Zr/10 diagram (Fig. 13c) whose success rate is within 0%–9.3% (Verma and Armstrong-Altrin 2016). In this diagram, except for sample S-11, all the Tadpatri shales are well plotted within the field of the continental arc.

There are several previous works that focused on basin evolution and tectonism of the Cuddapah basin. Based on fault pattern (transfer faults) and kinematic history, Chetty (2011) proposed that the development of Cuddapah basin is genetically related with Proterozoic collisional process. Sesha Sai et al. (2017) also suggest a continental arc setting during the evolution of the lower Cuddapah Group of rocks (Papaghini and Chitravati Group). Therefore the finding concluded from analyzing the above discussed tectonic discriminant diagrams is very much similar with the previous works.

5.3 Paleoredox conditions

The bivariate plot, SiO_2 versus ($Al_2O_3 + Na_2O + K_2O$) (Fig. 14a; Suttner and Dutta 1986) is applied to depict the climatic situation during Tadpatri clastic sedimentation. Most of the Tadpatri shale samples (except S-11) are well fitted in the area of semiarid climate, suggesting their deposition principally in semiarid condition.

Trace elements like U, Th, Cu, Zn, Ni, Co, V, Cr play a crucial role in interpreting the paleoredox condition. Sediment deposited in oxidizing environment mostly has a low

content of U, whereas those are deposited in oxygen minimum zone (OMZ) reflect higher content of U (Somayajulu et al. 1994; Madhavaraju and Ramasamy 1999; Armstrong-Altrin et al. 2015a; Ramos-Vázquez et al. 2017). Therefore the low U content (average 2.84 ppm) of the Tadpatri shale samples suggest that deposition of the Tadpatri formation is in an oxygenated condition. A U/Th ratio lower than 1.25 suggests oxidizing depositional condition and a value greater than 1.25 indicates deposition in a suboxic to anoxic environment (Nath et al. 1997). As the U/Th ratio of the Tadpatri shale samples (0.13–0.39 with an average 0.20; Table 2) is less than 1.25, it also indicates the deposition of clastic sediments in an oxic condition. A Cu/Zn ratio with a higher value indicates sediment deposition in a reducing environment, whereas the lower value supports an oxic environment (Nagarajan et al. 2007). In Tadpatri shale samples, the Cu/Zn ratio ranges between 0.19 and 1.94, with the average value of 0.66 (Table 2), which reveals a dominantly oxic condition during deposition, whereas a wide variation (low to moderate) in Cu/Zn ratio implies a fluctuating oxic condition (Oxic to slightly sub-oxic), possibly as a result of sea level shifting in Post-Archean period (Mir 2015). A Ni/Co ratio is also used to infer the depositional condition. All the analyzed samples have less than 5 Ni/Co ratios (average 2.22; Table 2), which indicates an oxic condition during deposition. Vanadium is commonly associated with the sediment as those are deposited in reducing condition, whereas Cr association within the sediment is not effected by redox condition (Dill 1986; Mir 2015). Therefore a V/Cr ratio greater than 4.25, within 2.00–4.25 and less than 2.00 indicates suboxic to anoxic, dyoxic and oxic environments, respectively (Jones and Manning 1994). Also, a V/(V + Ni) ratio higher than 0.84 suggests an euxinic condition, 0.54–0.82 represents an anoxic condition and 0.46–0.60 represents a dysoxic condition (Rimmer 2004; Mir 2015). A comparative study of V/Cr in between Tadpatri shale samples and PAAS showing relatively lesser values of the Tadpatri shale samples and implies oxic depositional environment (Fig. 2). Therefore based on this study it can said that the Ni/Co and V/Cr ratios (Fig. 14b) of Tadpatri shales suggests an oxic condition whereas the Ni/Co and V/(V + Ni) ratios (Fig. 14c) indicates that deposition is in an oxic to anoxic condition.

6 Conclusions

The geochemical signatures of clastic sedimentary rocks from Palaeo-Mesoproterozoic Tadptari formation provide important information about provenance, degree of paleoweathering and paleoredox condtions.

The CIA, PIA, CIW ratios of the Tadpatri shale samples indicate intense chemical weathering of the source rock. Based on chemical composition of Al_2O_3, K_2O and Na_2O illite is considered as most common clay mineral within the Tadpatri shales.

The Al_2O_3/TiO_2 ratio, the REE pattern, the trace elemental ratio (La/Sc, Th/Sc, Th/Co, La/Co), and the La/Sc versus Th/Co, Ni versus TiO_2, Zr versus TiO_2 plot reveal that the Tadpatri shales are principally derived from felsic source rocks. A mixed rock of 65% granite, 25% tonalite and 10% granodiorite of Eastern Dharwar Craton is proposed as the source rock of Tadpatri shales.

The trace-elemental signatures (U, U/Th, Ni/Co, V/Cr) imply the deposition of Tadpatri formation in an oxic environment. The wide range of Cu/Zn ratios of the Tadpatri shales implies that depositional environment fluctuates between oxidizing to sub-oxidizing conditions, possibly as a result of sea level change in Post-Archean period.

Acknowledgements The authors are grateful to the Department of Science and Technology (DST), Government of India for financial support vide PURSE (Phase-II) program (No. F4/SC/20/15) and University Grants Commission (UGC), New Delhi for the scholarship of the first author. Analyses of the major oxides and Trace, REE are performed at National Centre for Earth Science Studies, Thiruvananthapuram, Kerala and National Geophysical Research Institute, Hyderabad respectively. The authors are thankful to the Directors of these institutions. The authors are also grateful to Dr. C. Manikyamba, Senior Principal Scientist, NGRI and Dr. Sisir Mondal, Professor, Jadavpur University for their whole hearted support. Sincere thanks are also being accorded to Dr. J. S. Armstrong-Altrin and an anonymous reviewer for their constructive comments.

References

Absar N, Nizamudheen BM, Augustine S, Managave S, Balakrishnan S (2016) C, O, Sr and Nd isotope systematics of carbonates of Papaghini sub basin, Andhra Pradesh, India: implications for genesis of carbonate-hosted stratiform uranium mineralisation and geodynamic evolution of the Cuddapah basin. Lithos 263:88–100

Allen P (1985) The geochemistry of the Amphibolite-Granulite facies transition in Central South India (Ph.D. thesis). New Mexico Institute of Mining and Technology, Socorro, New Mexico, USA

Amajor LC (1987) Major and trace element geochemistry of Albian and Turonian shales from the Southern Benue trough, Nigeria. J Afr Earth Sci 6:633–641

Anand M, Gibson SA, Subbarao KV, Kelley SP, Dickin AP (2003) Early proterozoic melt generation processes beneath the intra cratonic Cuddapah basin, Southern India. J Petrol 44:2139–2171

Armstrong-Altrin JS (2009) Provenance of sands from Cazones, Acapulco, and Bahía Kino beaches, Mexico. Revista Mexicana de Ciencias Geológicas 26(3):764–782

Armstrong-Altrin JS (2015) Evaluation of two multidimensional discrimination diagrams from beach and deep-sea sediments from the Gulf of Mexico and their application to Precambrian clastic sedimentary rocks. Int Geol Rev 57(11–12):1446–1461

Armstrong-Altrin JS, Verma SP (2005) Critical evaluation of six tectonic setting discrimination diagrams using geochemical data of Neogene sediments from known tectonic settings. Sediment Geol 177(1–2):115–129

Armstrong-Altrin JS, Lee YI, Verma SP, Ramasamy S (2004) Geochemistry of sandstones from the upper Miocene Kudankulam formation, southern India: implications for provenance, weathering, and tectonic setting. J Sediment Res 74(2):285–297

Armstrong-Altrin JS, Lee YI, Kasper-Zubillaga JJ, Carranza-Edwards A, Garcia D, Eby N, Balaram V, Cruz-Ortiz NL (2012) Geochemistry of beach sands along the western Gulf of Mexico, Mexico: implication for provenance. Chemie der Erde-Geochemistry 72:345–362

Armstrong-Altrin JS, Machain-Castillo ML, Rosales-Hoz L, Carranza-Edwards A, Sanchez-Cabeza JA, Ruíz-Fernández AC (2015a) Provenance and depositional history of continental slope sediments in the Southwestern Gulf of Mexico unraveled by geochemical analysis. Cont Shelf Res 95:15–26

Armstrong-Altrin JS, Nagarajan R, Balaram V, Natalhy-Pineda O (2015b) Petrography and geochemistry of sands from the Chachalacas and Veracruz beach areas, western Gulf of Mexico, Mexico: constraints on provenance and tectonic setting. J S Am Earth Sci 64:199–216

Armstrong-Altrin JS, Lee YI, Kasper-Zubillaga JJ, Trejo-Ramírez E (2017) Mineralogy and geochemistry of sands along the Manzanillo and El Carrizal beach areas, Southern Mexico: implications for palaeoweathering, provenance, and tectonic setting. Geol J 52(4):559–582

Bhatia MR (1983) Plate tectonics and geochemical composition of sandstones. J Geol 91:611–627

Bhatia MR, Crook KAW (1986) Trace element characteristics of graywackes and tectonic setting discrimination of sedimentary basins. Contrib Miner Petrol 92(2):181–193

Chakrabarti G, Shome D, Bauluz B, Sinha S (2009) Provenance and weathering history of Mesoproterozoic clastic sedimentary rocks from the basal Gulcheru formation, Cuddapah basin, India. J Geol Soc India 74:119–130

Chetty TRK (2011) Tectonics of Proterozoic Cuddapah basin, Southern India: a conceptual model. J Geol Soc India 78:446–456

Condie KC (1993) Chemical composition and evolution of the upper continental crust: contrasting results from surface samples and shales. Chem Geol 104:1–37

Cox R, Low DR, Cullers RL (1995) The influence of sediment recycling and basement composition on evolution of mudrock chemistry in the southwestern United States. Geochim Cosmochim Acta 59:2919–2940

Cullers RL (1995) The controls on major and trace element evolution of shales, siltstones, and sandstones of Ordovician to Tertiary age in the Wet Mountains region, Colorado, USA. Chem Geol 123:107–131

Cullers RL (2000) The geochemistry of shales, siltstones and sandstones of Pennsylvanian–Permian age, Colorado, USA: implications for provenance and metamorphic studies. Lithos 51:181–203

Cullers RL (2002) Implications of elemental concentrations for provenance, redox conditions, and metamorphic studies of shales and limestones near Pueblo, CO, USA. Chem Geol 191(4):305–327

Cullers RL, Podkovyrov VN (2000) Geochemistry of Mesoproterozic Lakhanda shales in southeastern Yakutia, Russia: implications for mineralogical and provenance control and recycling. Precambrian Res 104:77–93

Dill H (1986) Metallogenesis of Early Paleozoic graptolite shales from the Graefenthal Horst (northern Bavaria-Federal Republic of Germany). Econ Geol 81:889–903

Fedo CM, Nesbitt HW, Young GM (1995) Unraveling the effects of K-metasomatism in sedimentary rocks and paleosols, with implications for paleoweathering conditions and provenance. Geology 23:921–924

Fedo CM, Eriksson K, Krogstad EJ (1996) Geochemistry of shale from the Archean (~ 3.0 Ga) Buhwa Greenstone belt, Zimbabwe: implications for provenance and source area weathering. Geochim Cosmochim Acta 60(10):1751–1763

Floyd PA, Winchester JA, Park RG (1989) Geochemistry and tectonic setting of Lewisian clastic metasediments from the Early Proterozoic Loch Maree Group of Gairloch, NW Scotland. Precambrian Res 45:203–214

French JE, Heaman LM, Chacko T, Srivastava RK (2008) 1891–1883 Ma Southern Bastar–Cuddapah mafic igneous events India: a newly recognized large igneous province. Precambrian Res 160:308–322

Harnois L (1988) The CIW index: a new chemical index of weathering. Sediment Geol 55:319–322

Hayashi K, Fujisawa H, Holland HD, Ohmoto H (1997) Geochemistry of ~ 1.9 Ga sedimentary rocks from northeastern Labrador, Canada. Geochimica et Cosmochimica Acta 61:4115–4137

Herron MM (1988) Geochemical classification of terrigenous sands and shales from core or log data. J Sediment Pet 58(5):820–829

Hessler AM, Lowe DM (2006) Weathering and sediment generation in the Archean: an integrated study of the evolution of siliciclastic sedimentary rocks of the 3.2 Ga Moodies Group, Barberton Greenstone Belt, South Africa. Precambrian Res 151:185–210

Jayananda M, Moyen JF, Martin H, Peucat JJ, Auvray B, Mahabaleswar B (2000) Late Archaean (2550–2520 Ma) juvenile magmatism in the Eastern Dharwar craton, Southern India: constraints from geochronology, Nd–Sr isotopes and whole rock geochemistry. Precambrian Res 99:225–254

Jones B, Manning DC (1994) Comparison of geochemical indices used for the interpretation of paleo-redox conditions in ancient mudstones. Chem Geol 111(1–4):111–129

Kale V (1991) Constraints on the evolution of the Purana basins of peninsular India. J Geol Soc India 38:231–252

Khelen AC, Manikyamba C, Ganguly S, Singh T, Subramanyam KSV, Ahmad SM, Reddy MR (2017) Geochemical and stable isotope signatures of Proterozoic stromatolitic carbonates from the Vempalle and Tadpatri formations, Cuddapah Supergroup, India: implications on paleoenvironment and depositional conditions. Precambrian Res 298:365–384

Li DF, Chen HY, Li Z, Fralick P, Hollings P, Mi M, Lu WJ, Han JS, Wang CM, Fang J (2017) Geochemistry of fine-grained clastic rocks in the Mesoproterozoic Kawabulake Group: implications for provenance and the tectonic model of the Eastern Tianshan, Xinjiang, NW China. Int J Earth Sci 106:115–129

Long XP, Yuan C, Sun M, Safonova I, Xiao WJ, Wang YJ (2012) Geochemistry and U–Pb detrital zircon dating of Paleozoic graywackes in Junggar, NW China: insights into subduction accretion processes in the southern Central Asian Orogenic Belt. Gondwana Res 21:637–653

Madhavaraju J, Ramasamy S (1999) Rare earth elements in limestones of Kallankurichchi Formation of Ariyalur Group, Tiruchirapalli Cretaceous, Tamil Nadu. J Geol Soc India 54:291–301

Manikyamba C, Kerrich R, González-Álvarez I, Mathur R, Khanna TC (2008) Geochemistry of Paleoproterozoic black shales from the Intracontinental Cuddapah basin, India: implications for provenance, tectonic setting, and weathering intensity. Precambrian Res 162:424–440

McLennan SM (1993) Weathering and global denudation. J Geol 101(2):295–303

McLennan SM, Hemming S, McDaniel DK, Hanson GN (1993) Geochemical approaches to sedimentation, provenance and tectonics. In: Johnson MJ, Basu A (eds) Processes controlling the composition of clastic sediments, vol 284. Geological society of America, Boulder, pp 21–40 **(Special Paper)**

Mir AR (2015) Rare earth element geochemistry of Post- to Neo-archean shales from Singhbhum mobile belt, Eastern India: implications for tectonic setting and paleo-oxidation conditions. Chin J Geochem 34(3):401–409

Mishra DC (2011) Long hiatus in Proterozoic sedimentation in India: Vindhyan, Cuddapah and Pakhal basins—a plate tectonic model. J Geol Soc India 77:17–25

Murthy YGK, Babu Rao V, Guptasarma D, Rao JM, Rao MN (1987) Tectonic and petrochemical and geophysical studies of mafic dyke swarns around the Proterozoic Cuddapah basin, South India. In: Halls HC, Fahrig WF (eds) Mafic dyke swarms, vol 34. Geological Association of Canada, St John's, pp 303–317 **(Special papers)**

Nagaraja Rao BK, Rajurkar ST, Ramalingaswami G, Ravindra BB (1987) Stratigraphy, structure and evolution of Cuddapah basin. In: Radhakrishna BP (ed) Purana basins of Peninsular India, vol 6. Geological Society of India, Bangalore, pp 33–86 **Bulletins**

Nagarajan R, Madhavaraju J, Nagendra R, Armstrong-Altrin JS, Moutte J (2007) Geochemistry of Neoproterozoic shales of Rabanpalli formation, Bhima basin, Northern Karnataka, Southern India: implications for provenance and paleo-redox conditions. Revista Mexicana de Ciencias Geológicas 24(2):150–160

Nagarajan R, Roy PD, Jonathan MP, Lozano R, Kessler FL, Prasanna MV (2014) Geochemistry of Neogene sedimentary rocks from Borneo basin, East Malaysia: paleo-weathering, provenance and tectonic setting. Chem Erde 74:139–146

Nath BN, Bau M, Ramalingeswara Rao B, Rao CHM (1997) Trace and rare earth elemental variation in Arabian Sea sediments through a transect across the oxygen minimum zone. Geochim Cosmochim Acta 61(12):2375–2388

Nesbitt HW, Young GM (1982) Early Proterozoic climates and plate motions inferred from major element chemistry of lutites. Nature 299:715–717

Nesbitt HW, Young GM (1984) Prediction of some weathering trends of plutonic and volcanic rocks based on thermodynamic and kinetic considerations. Geochim Cosmochim Acta 48:1523–1534

Patranabis-Deb S, Saha D, Tripathy V (2012) Basin stratigraphy, sea-level fluctuations and their global tectonic connections—evidence from the Proterozoic Cuddapah basin. Geol J 47:263–283

Pettijohn FJ (1975) Sedimentary rocks, 3rd edn. Harper and Row, Publishers, New York, p 628

Ramos-Vázquez M, Armstrong-Altrin JS, Rosales-Hoz L, Machain-Castillo ML, Carranza-Edwards A (2017) Geochemistry of deep-sea sediments in two cores retrieved at the mouth of the Coatzacoalcos river delta, Western Gulf of Mexico, Mexico. Arab J Geosci 10(6):148

Rimmer SM (2004) Geochemical paleoredox indicators in Devonian–Mississippian black shales, central Appalachian basin (USA). Chem Geol 206:373–391

Roser BP, Korsch RJ (1986) Determination of tectonic setting of sandstone-mudstone suites using SiO_2 content and K_2O/Na_2O ratio. J Geol 94(5):635–650

Saha D, Tripathy V (2012) Paleoproterozoic sedimentation in the Cuddapah basin, South India and regional tectonics: a review. In: Majumder R, Saha D (eds) Paleoproterozoic of India. Geological Society of London, London, pp 161–184 **(Special Publication)**

Sesha Sai VV, Tripathy V, Bhattacharjee S, Khanna TC (2017) Paleoproterozoic magmatism in the Cuddapah basin, India. J Indian Geophys Union 21(6):516–525

Sharma M, Shukla M (2003) Studies in Palaeo–Mesoproterozoic stromatolites from Vempalle and Tadpatri formations of Cuddapah Supergroup, India. In: Vistas in Palaeobotany and Plant Morphology: evolutionary and environmental perspectives (Professor D.D. Pant Memorial Volume), pp 1–25

Somayajulu BLK, Yadav DN, Sarin MM (1994) Recent sedimentary records from the Arabian Sea. Proc Indian Acad Sci Earth Planet Sci 103(2):315–327

Spalletti LA, Queralt I, Matheos SD, Colombo F, Maggi J (2008) Sedimentary petrology and geochemistry of siliciclastic rocks from the upper Jurassic Tordillo formation (Neuquen basin, western Argentina): implications for provenance and tectonic setting. J S Am Earth Sci 25:440–463

Sun L, Gui H, Chen S (2013) Geochemistry of sandstones from the Neoproterozoic Jinshanzhai formation in northern Anhui Province, China: provenance, weathering and tectonic setting. Chin J Geochem 32(1):95–103

Suttner LJ, Dutta PK (1986) Alluvial sandstones composition and paleoclimate, I. Framework mineralogy. J Sediment Res 56(3):329–345

Tapia-Fernandez HJ, Armstrong-Altrin JS, Selvaraj K (2017) Geochemistry and U–Pb geochronology of detrital zircons in the Brujas beach sands, Campeche, Southwestern Gulf of Mexico, Mexico. J S Am Earth Sci 76:346–361

Taylor SR, McLennan SM (1985) The continental crust: its composition and evolution. Blackwell Scientific, Oxford, p 312

Verma SP, Armstrong-Altrin JS (2013) New multi-dimensional diagrams for tectonic discrimination of siliciclastic sediments and their application to Precambrian basins. Chem Geol 355:117–133

Verma SP, Armstrong-Altrin JS (2016) Geochemical discrimination of siliciclastic sediments from active and passive margin settings. Sediment Geol 332:1–12

Wronkiewicz DJ, Condie KC (1987) Geochemistry of Archean shales from the Witwatersrand Supergroup, South Africa: source area weathering and provenance. Geochim Cosmochim Acta 51:2401–2416

Zachariah JK, Bhaskar Rao YJ, Srinivasan R, Gopalan K (1999) Pb, Sr and Nd isotope systematics of uranium mineralised stromatolitic dolomites from the Proterozoic Cuddapah Supergroup, South India: constraints on age and provenance. Chem Geol 162:49–64